Optical Fiber Technology 66 (2021) 102638

Contents lists available at ScienceDirect

Optical Fiber Technology

journal homepage: www.elsevier.com/locate/yofte

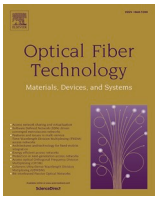

Dip coating of thin polymer optical fibers

Andreas Evertz *, Daniel Schrein, Ejvind Olsen, Gerd-Albert Hoffmann, Ludger Overmeyer

Leibniz Universität Hannover, Institute of Transport and Automation Technology, An der Universität 2, 30823 Garbsen, Germany

ARTICLE INFO

Keywords:
Polymer optical fiber
Continuous dip coating
Extruded optical fibers

ABSTRACT

To produce polymer optical fibers in research environments, a flexible cladding material-application process is required. Further, to functionalize the waveguide, the fiber core-production step needs to be separated from the cladding application, contrasting conventional polymer optical fiber production processes. In this study, we developed a solution using continuous dip-coating technique to apply cladding material onto previously extruded polymer optical fiber cores with diameters as low as 16 μm. The process was designed considering the fluid-dynamic behavior of the cladding material and fiber to achieve a radially symmetric coating thickness. We examined UV-curable resin as cladding and polymethyl-methacrylate (PMMA)-based extruded optical fibers with diameters of up to 16 μm. The proposed method helped continuously coat optical fiber cores with cladding material with diameters in the range of 1 mm and achieve the lowest optical attenuation (<3 dB/m).

1. Introduction

Polymer optical fibers (POFs) are used in various applications, such as audio transmission and stress sensing, owing to their superior mechanical stability. Moreover, standard POFs, with a diameter of 1 mm, are easier to install and operate than conventional glass optical fibers are. Nevertheless, POFs are not widely used because of their higher attenuation than that of glass fibers. Thus, they are only viable for short-range data-transmission applications with transmission rates of nearly 40 Gbit/s, which have been achieved for a graded-index POF with a length of 50 m [1].

The co-extrusion process is a state-of-the-art production standard for POFs, in which the fiber cores and cladding structures are produced simultaneously using two extruders [2]. Dip-coating processes are widely used in applications where homogenous coating thicknesses need to be achieved. The application of POF dip coating is predominantly discontinuous, enabling the generation of polymer fiber sensors using a variety of appropriate coating materials [3,4]. A commonly used material for POFs is polymethyl methacrylate (PMMA), which has low attenuation in the visible wavelength spectrum and low manufacturing costs. The lowest attenuation achieved for a PMMA-based POF is 20 dB/km at 650–680 nm [6]. When transmitting light in the infrared range, a higher attenuation is primarily caused by the carbon-hydrogen bonds in the polymer. Thus, by exchanging hydrogen with substances such as fluorine, the attenuation of a POF can be reduced. A low-loss POF, Lucina™, was synthesized using a perfluorinated polymer called CYTOP®, which exhibited an attenuation of 10 dB/km at a wavelength of 1000 nm [2].

In this study, we extruded the POF core and applied the cladding using a continuous dip-coating process in two separate production steps. Unlike conventional fiber production processes [5], the separated process steps enable a versatile process for laboratory environments, flexible examination of different optical material combinations, and intermediate treatment of fiber cores. Thus, POF sensors can be implemented by introducing gratings to the core fibers. While the laser-inscription process of fiber Bragg gratings (FBGs) in PMMA fibers is time consuming, faster inscription times can be achieved by either doping PMMA with a photosensitive material or via etching. Both procedures can also be applied simultaneously for faster inscription times [7]. Using the intermediate inscription, the time and energy consumption for creating FBGs in undoped PMMA POFs can be potentially reduced. In this study, a self-centering effect, originating from the forces applied to the fiber, is attempted to be implemented to improve the POF practicality. Aiming on cladded fiber diameter of 1 mm, the handling advantage of a large POF can be used together with fiber core diameters in the single-mode range. The centered position of the smaller fiber core is particularly important for the application of POFs, whereas the alignment of two fiber cores is crucial for sufficient functionality.

* Corresponding author.
E-mail address: andreas.evertz@ita.uni-hannover.de (A. Evertz).

https://doi.org/10.1016/j.yofte.2021.102638
Received 6 April 2021; Received in revised form 22 June 2021; Accepted 9 July 2021
Available online 15 July 2021
1068-5200/© 2021 The Author(s). Published by Elsevier Inc. This is an open access article under the CC BY license (http://creativecommons.org/licenses/by/4.0/).

2. Experimental work

2.1. Dip-coating process

Dip-coating processes are used to coat structures with a fluid material, which is then solidified either by curing the material itself or evaporating an additional solvent [8]. Subsequently, we used the dip-coating process to apply the UV-curable cladding onto polymer fiber cores, which were manufactured using our fiber extruder system. Fig. 1 represents a schematic of forces occurring in the dip-coating of circular fibers. The fiber path is redirected around a rod inside the liquid, which causes the fiber to pass out of the liquid perpendicular to its surface. The inertia of the fiber is transferred to the liquid at the surface of the fiber, where due to the adhesion of the fluid to the fiber surface, no relative fluid velocity (Dirichlet boundary condition) appeals. Consequently, the liquid resin is accelerated along the fiber, forming a meniscus on the resin surface. The thickness of the meniscus *D* depends on dipping length *L*, fiber velocity *v*, and liquid properties, such as viscosity and density. Different equations can be used to calculate final coating thickness *d* for different dip-coating settings [9,10]. The fundamental behavior of dip-coating thicknesses are higher at drawing speeds lower than 0.1 mm/s and higher than 1 mm/s, whereas thicknesses are the lowest when the viscosity are the highest and drawing velocities are medium [11].

As shown in Fig. 1, different forces acting on the fiber opposed to the drawing direction during the process are $\overrightarrow{F_G}$, gravitational force of the adhering resin; $\overrightarrow{F_I}$, inertial (inner friction) force owing to the inertia of the resins; and $\overrightarrow{F_F}$, retracting friction force caused by fiber guiding components. All these forces are in equilibrium with drawing force $\overrightarrow{F}$ applied to the fiber in the drawing direction. This sum of forces becomes a significant factor in the dip-coating process of thin polymer fibers and must be lower than the tensile strength of the fiber itself to prevent failures in the process. As $\overrightarrow{F_I}$ is the same in every perpendicular direction along the fiber, theoretically, a radially symmetric meniscus evolves around the fiber. This enables a radial homogenous coating thickness with the gravitational force being opposed to the drawing direction, leading to the fiber core self-centering in the coated POF.

A considerable phenomenon occurring during the dip coating of fibers is the Plateau-Rayleigh instability [9]. This phenomenon causes a fluid driven by surface tension to form periodic droplets on the fiber, which must be avoided to achieve uniform coating wetting. The Plateau-Rayleigh instability is affected mainly by the viscosity of coating and the time that the fluid has to form droplets. Increasing the resin temperature and fiber drawing speed yields higher viscosities and rapid curing that can overcome the Plateau-Rayleigh instability.

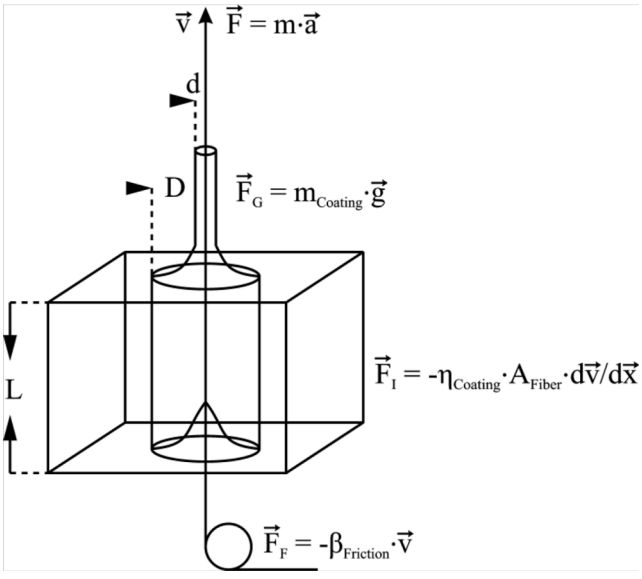

Fig. 1. Schematic representation of the forces applied to the fiber in the dip-coating process.

2.2. Material selection

The fiber cores were extruded with PMMA POQ 62 granulate (Evonik Performance Materials GmbH) using a piston extruder. This core material has a refractive index of $n_{core} = 1.49$ and enables fiber diameters ranging from 10 to 70 μm in our extrusion process. As an optically compatible coating, PC 409 with a refractive index of $n_{coating} = 1.4$ (Fospia/Efiron) was used. The viscosity of coating resin was measured with respect to temperature (Fig. 2).

The viscosity was measured at a shear rate of 1 s^{-1} as the shear rate during the dip-coating process is comparable. The black curve is obtained using the Arrhenius equation, as follows:

$$\eta(T) = \eta_0 * \exp\left(\frac{E_A}{R * T}\right) \quad (1)$$

where T is the temperature, η_0 is a material constant, R is the universal gas constant, and E_A is the activation energy. The following parameters were calculated:$\eta_0 = 1,36*10^{-8}$ mPa*s and $E_A = 6,31*10^4$ J.

2.3. Experimental setup

We designed a dip-coating setup to coat the PMMA fiber cores, as shown in Fig. 3. The fiber cores were previously extruded onto a spool that can be used directly at the unwinder. From the unwinder, the fiber is drawn through the coating resin tub, where it is redirected perpendicular to the resin surface, and through the UV hardening unit, where the liquid coating is cured. Finally, the fiber is collected by the winder at the top, which is controlled to rotate with the same tangential speed as the unwinder to achieve low to zero traction on the fiber. To start the process, the polymer fiber is fixed to a 50-μm copper fiber, which can be easily guided through each process step owing to its higher strength. By attaching the copper fiber to the top winder, the initial fiber core end is pulled through each process step.

The dip-coating bath can be heated or cooled to adjust the viscosity of the resin. Therefore, the temperature-control unit uses thermal conduction by attaching to the bottom plate of the resin tub. The temperature is controlled by a control unit using thermal sensors attached to the bottom of the resin tub. The side walls of the bath are designed to

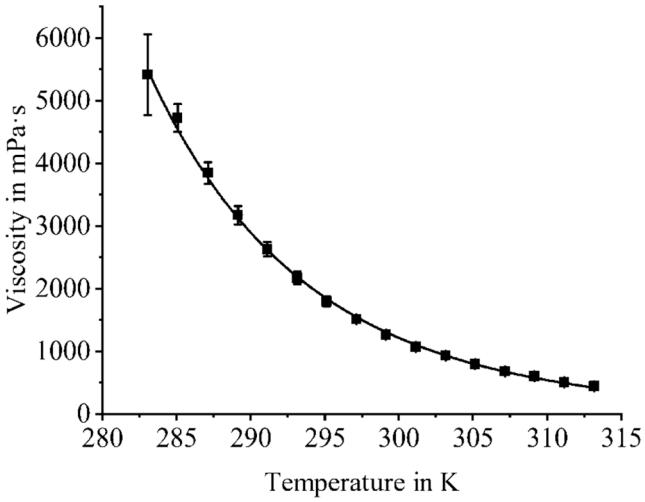

Fig. 2. Viscosity of the coating resin measured with a rotary viscosimeter (MCR 302) at different temperatures for a shear rate of 1 s^{-1}.

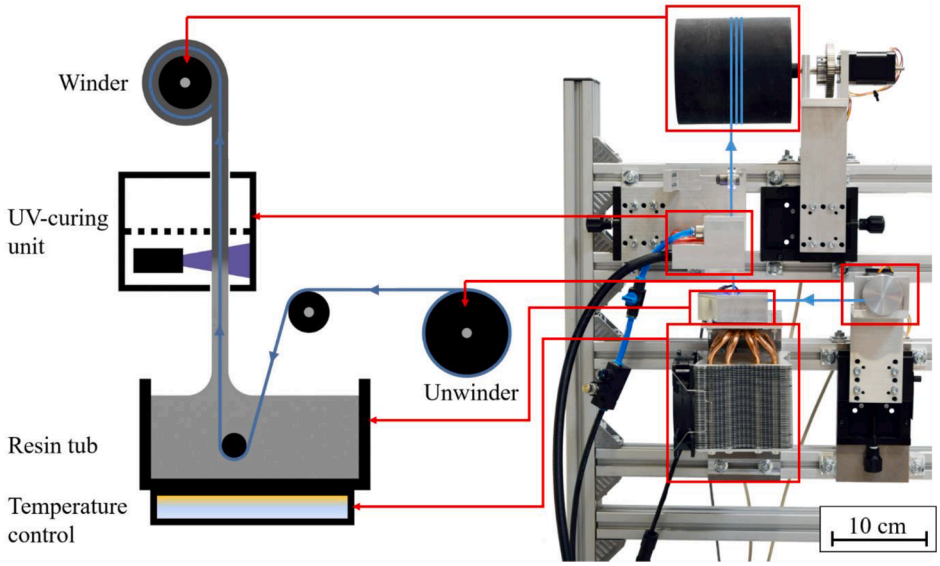

Fig. 3. Setup of the dip-coating system with the fiber path marked in blue.

maintain a minimum distance of 40 mm from the fiber. Thus, the fluid-dynamic influence of the walls on the coating process is minimized. This distance was calculated using an estimation with the equation for inertial force $\vec{F_I}$ of the resin being approximately zero (Fig. 1). The guiding rod shown in Fig. 4 has a groove with a depth of 0.5 mm, which maintains the fiber in its designated position. The 3-mm guiding rod is placed 2 mm above the bottom of the tub; thus, the unperturbed coating process starts at a height greater than 5 mm. In the curing unit, subsequent to the coating unit, the goal is to avoid oxidation. Therefore, the UV encasing, where the curing takes place, is filled with nitrogen, which is distributed through a chamber located on top of the UV encasing. Through evenly distributed holes between the nitrogen chamber and UV encasing, nitrogen is guided homogenously into the UV encasing. These holes are supposed to reduce turbulence, which can introduce vibrations into the fiber and thus affect the coating-process stability. A broadband source (OmniCure S1500, 320–500 nm) with an output power of 200 W is used as the UV curing source. The curing unit is placed 57 mm above the guiding rod inside the resin bath. According to a preliminary investigation, this position represents the farthest possible distance between the resin bath and curing unit to avoid the Plateau-Rayleigh instability and interference with the meniscus.

3. Results

To characterize the coating resin, we measured the coating thickness under variations of drawing velocity and resin temperature. First, the experiments were conducted using a copper fiber core with a diameter of 50 µm to avoid experimental deviations owing to the fluctuating extruded fiber diameter. Fig. 5 demonstrates the measurement results, in which the black dots indicate the measurement parameters. The diameter was measured with a digital calibrated microscope using a built-in distance measurement tool, with a measurement error of ± 5 µm. Each fiber in this chapter was measured at four positions with a distance of 80 mm from each other, where the coating had already been fully formed.

In Fig. 5, three different parameter spaces are visible, limiting the possible dip-coating settings. It is only possible to apply the coating resin onto the fiber in Area II. In area I, the drawing velocity was comparably slow, and Plateau-Rayleigh instabilities occurred. In area III, the coating thickness was too high, and the resin coating could not be cured entirely. In general, the coating thickness increases as drawing velocity and

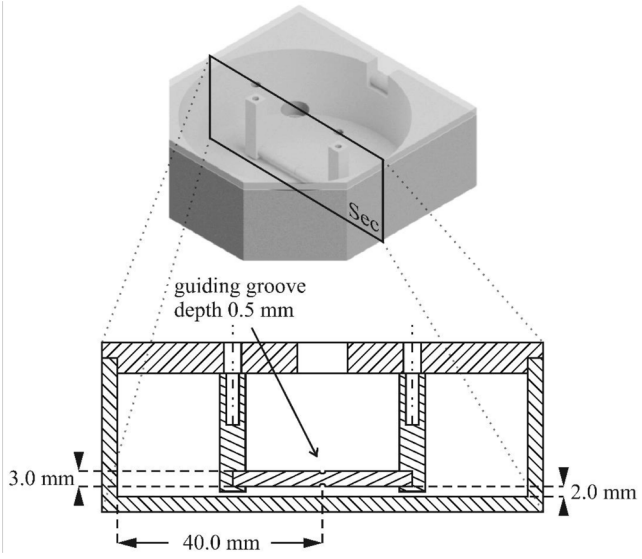

Fig. 4. Three-dimensional (3D) model and cross-section of the resin tub used for dip coating.

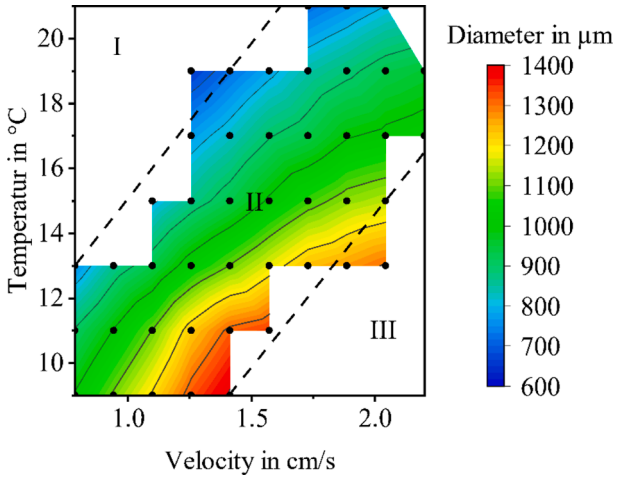

Fig. 5. Contour plot showing the coated copper fiber diameters by variation of the resin temperature and drawing velocity of the fiber.

temperature-induced viscosity increase. Because of the shorter UV exposure time, the coating softens at higher velocities. To utilize a stable process parameter setting, we chose a drawing velocity of 0.15 cm/s and temperature of 16 °C for further measurements, which resulted in a fully hardened coating with a diameter of approximately 1 mm.

The dependence of the fill level of the dip-coating bath on the coated fiber diameter is shown in Fig. 6. In three repeated measurements (M.1–M.3), a drastic decrease in the coated fiber diameter was observed for fill levels under 6 mm. This is caused by the construction of the resin tub (Fig. 4), in which the guiding rod is located at a height of 5 mm, interfering with the coating process. The apparent decrease in the diameter for levels above 8 mm could be a result of a vertical temperature gradient in the resin tub. This temperature gradient occurs with increasing distance from the temperature-control unit; thus, when the resin tub is cooled, the temperature rises and viscosity decreases along the fiber drawing direction. Fig. 5 shows that the coating thickness decreases as the temperature increases.

The dependence of the total diameter of coating on the diameter of the extruded PMMA core fibers is shown in Fig. 7. In our experiments, PMMA cores were extruded at four different velocities prior to coating them. These four extrusion velocities resulted in different fiber diameters, which is the reason for the clustering of the measurement points around the core diameters of 33, 38, 43, and 48 µm. The error bars indicate the diameter fluctuations along the obtained fibers. The graph suggests a linear increase in the total coated fiber thickness with an increase in the core fiber diameter. Therefore, a line of best fit is drawn, showing a gradient of 3.36 $\mu m_{\text{total diameter}}/\mu m_{\text{core diameter}}$, which is close to π. This implies that because of the circular shape of the core fiber, the total coating diameter directly depends on the core circumference surface, which also increases with the factor π to the core diameter. As stated in Section 2.1, owing to the Dirichlet boundary condition at the surface of the core fiber, the inertia is transferred; thus, the amount of accelerated coating material increased and a larger total diameter was obtained.

In the following discussion, we showcase two coated PMMA fibers. Fig. 8 shows the first fiber that has a length of 2.3 m, a fiber core diameter at the front faces of $d_{core} = 45.7 \pm 0.5$ µm, and a total diameter of $d_{coating} = 1003.1 \pm 0.5$ µm (n = 32). Fig. 9 shows the second fiber, which is the thinnest fiber core that was coated with a diameter of $d_{core} = 16.1 \pm 0.5$ µm. As a consequence of the smaller diameter, the second fiber has a lower absolute strength; therefore, the resulting length of the coated fiber without breaking was 210 mm. The achieved coating diameter was $d_{coating} = 790.6 \pm 26.9$ µm. As stated

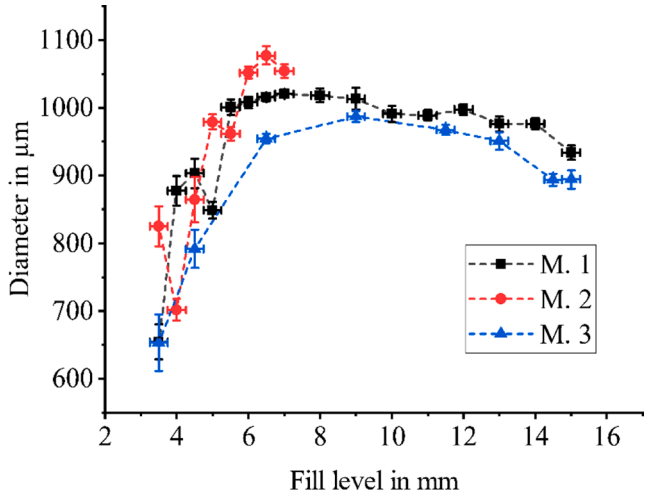

Fig. 6. Diameter of the resulting coated copper fiber for different resin fill levels of the resin tub with a drawing velocity of 0.15 cm/s and temperature of 16 °C.

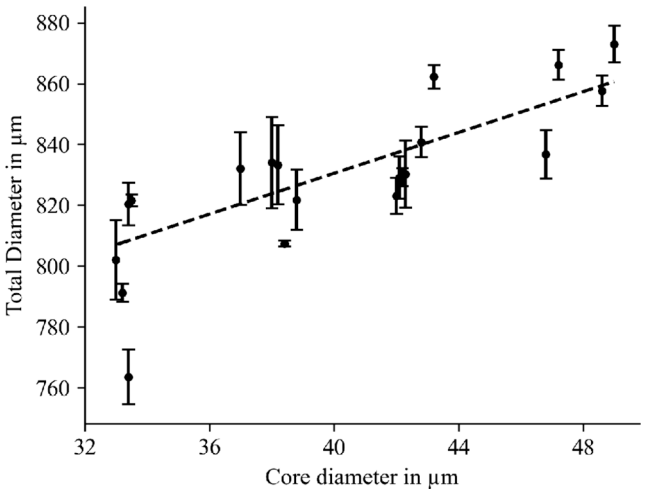

Fig. 7. Diameter of the resulting coated fiber for different extruded PMMA core diameters with a drawing velocity of 0.15 cm/s and temperature of 16 °C.

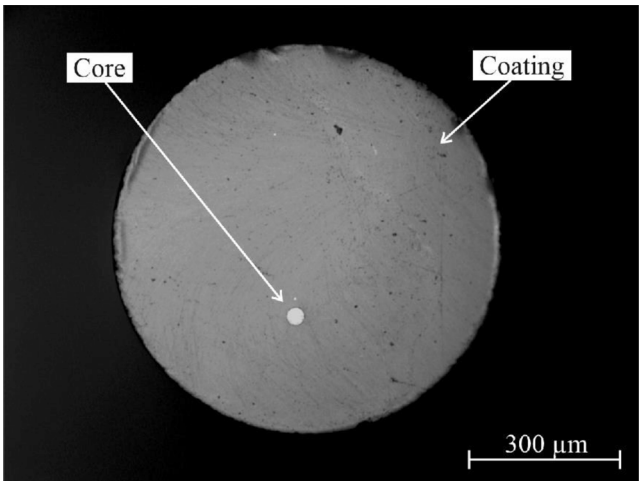

Fig. 8. Front face of the PMMA fiber embedded in coating with a core diameter of.45.7 ± 0.5 µm.

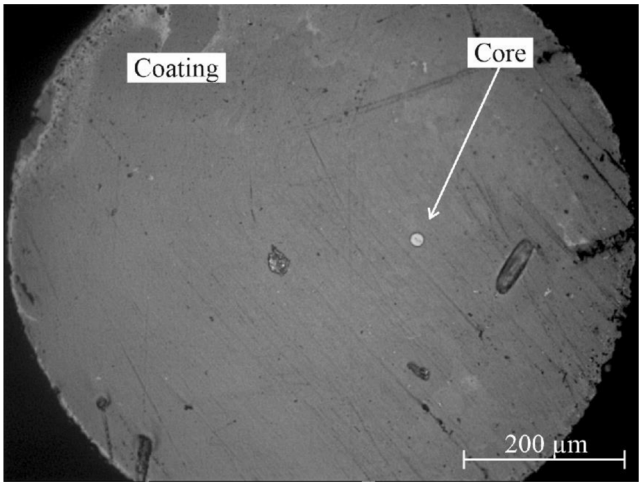

Fig. 9. Front face of the PMMA fiber embedded in coating with a core diameter of.16.1 ± 0.5 µm.

in Subsection 2.1, in theory, the core should center itself during the dip-coating process if it is moving antiparallel to the gravitational force. Nevertheless, it was observed in side view microscopy that the fiber core is decentered. Figs. 8 and 9 show exemplary cross-sections of differently sized fiber cores cladded with the same process parameters. For both core fiber diameters, circular cladding geometries develop because there is no shrinkage in the material. However, both fiber cores exhibit insufficient centering, which might be caused by the comparably low drawing speed resulting in low inertial forces in the coating or disturbing influences owing to the guiding of the fiber core.

Furthermore, the attenuation of the coated optical fibers was measured using a laser diode at a wavelength of 638 nm. At the fiber input, the system used cameras for alignment and an iris to change the beam diameter, allowing precise coupling into the fiber core. To examine the outcoupling light from the fiber, a camera with an adjustable numerical aperture was used in combination with a beam profiler and an Ulbricht sphere (Fig. 10). By sequentially positioning these tools in front of the fiber output surrounding, the light and cladding modes can be excluded from the power measurement; thus, only the optical power guided through the fiber core is measured. To analyze the attenuation behavior related to the length of the fiber, cut-back measurements were performed. The cut-back method includes a series of measurements of optical output power P_O with sequentially decreasing fiber lengths. Over the entire series of measurements, the input coupling remains intact; hence, input power P_I is maintained as a constant. Using this method, we could maintain constant input conditions throughout the measurement and thus neglect all power loss effects at the input facet of the fiber. Additionally, we could explore distribution of the attenuation along the fiber, which could vary in particular owing to the output facet quality. With these power measurements, the total attenuation was calculated for each fiber length.

The measured attenuations of the coated fiber with a core diameter of 45.7 ± 0.5 μm (Fig. 8) are shown in Fig. 11. We observe an increase in attenuation for longer fibers, suggesting a linear growth. Using the line of best fit, we achieve a gradient, which describes the mean attenuation based on the POF length of $\alpha_{\text{mean}} = 2.98$ dB/m, and a vertical intercept, which describes the total attenuation caused by the end facets of 0.03 dB. As a consequence of having a short length, only one measurement could be performed for the fiber with a core diameter of 16.1 ± 0.5 μm, as shown in Fig. 9, resulting in an attenuation of 17.3 dB/m. This higher attenuation can mainly be attributed to the lower quality of the thinner extruded fiber core and its smaller diameter, which leads to more interaction of the evanescent field with the cladding. The applied extrusion process used for the PMMA fiber core production is a possible source of fluctuations in the attenuation.

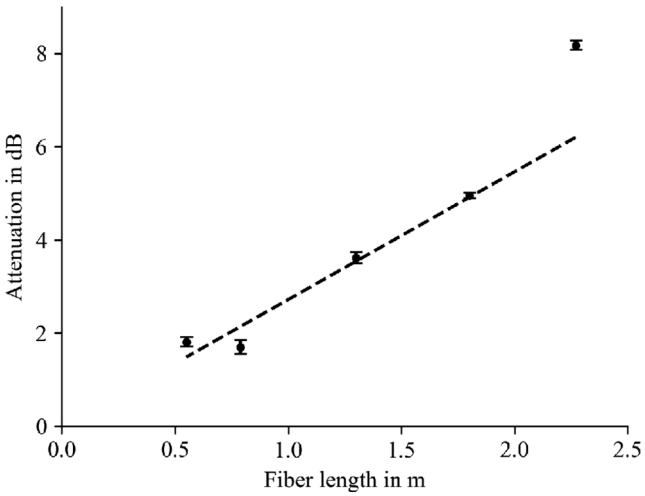

Fig. 11. Attenuation of the coated PMMA fiber core (core diameter = 45.7 ± 0.5 μm) using the cutback method.

4. Summary and outlook

In this study, we introduced a dip-coating system for applying cladding materials to extruded optical fiber cores. We developed a solution using a continuous dip-coating technique to apply cladding material onto previously extruded polymer optical fiber cores with diameters as low as 16 μm; however, to enable a stable and continuous process, the fiber needs to have a diameter of at least 20 μm. The best measured attenuations were close to 3 dB/m for fibers with a core diameter of 46 μm. The coating diameter was consistently correlated to the core fiber diameter and boundary surface. Because the resulting cladding thickness was completely above the evanescent field depth, the change in coating thickness did not affect the functionality of optical fibers. The proposed system is a flexible alternative to co-extrusion processes that can be applied in small-scale laboratory environments. Because a small amount of resin material is required, the proposed process can be used to examine new material combinations.

Our future study will focus on improving the production of fiber cores and increasing the drawing speed of fibers to achieve improved self-centering of the core and less Plateau-Rayleigh instability effect. Therefore, the coating system is adapted by incorporating the curing unit into the coating unit to minimize the fiber path between the steps. Furthermore, separation of the two production steps will be utilized with different treatments on the fiber cores before the coating process to investigate the sensor and lighting applications.

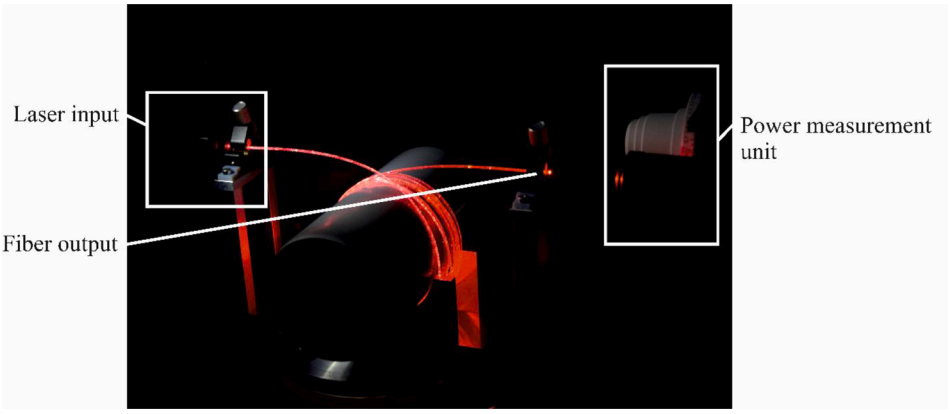

Fig. 10. Measurement setup to determine the optical attenuation with a red laser at a wavelength of 638 nm.

CRediT authorship contribution statement

Andreas Evertz: Validation, Writing - original draft, Visualization. **Daniel Schrein:** Investigation, Conceptualization, Writing - original draft. **Ejvind Olsen:** Visualization, Supervision. **Gerd-Albert Hoffmann:** Supervision, Funding acquisition. **Ludger Overmeyer:** Supervision, Funding acquisition, Project administration.

Declaration of Competing Interest

The authors declare that they have no known competing financial interests or personal relationships that could have appeared to influence the work reported in this paper.

Acknowledgments

This study was conducted within the LAPOF project. This work was supported by the Europäischer Fond für Regionale Entwicklung (EFRE) and the state Niedersachsen-Regionenkategorie Stärker Entwickelte Regionen (SER) under project number 85003655. The authors would like to thank Evonik Performance Materials GmbH for supplying the PMMA for the fiber cores, and Farbwerke Herkula SA/AG for supplying the coating material used in testing and optimizing the dip-coating system.

References

[1] S. Schoellmann, C. Wree, A. Joshi, et al., First experimental transmission over 50 m gi-pof at 40 gb/s for variable launching offsets, in: 33rd European Conference and Exhibition of Optical Communication - Post-Deadline Papers (published 2008), 2007, pp. 1–2.
[2] Y. Koike, Fundamentals of Plastic Optical Fibers, Wiley-VCH, Weinheim, Germany, 2015.
[3] Z. Mahmud, S.H. Herman, U.M. Noor, S. Saharudin, Performance characterization of optical fiber oxygen sensor in gas and aqueos phase, in: IEEE Student Conference on Research and Developement, 2013, pp. 569–571.
[4] S.K. Khijwania, K.L. Srinivasan, J.P. Singh, An evanescent-wave optical fiber relative humidity sensor with enhanced sensitivity, Sens. Actuators B: Chemical 104 (2) (2005).
[5] M. Beckers, T. Schlüter, T. Vad, T. Gries, C.-A. Bunge, An overview on fabrication methods for polymer optical fibers, Polym. Int. 64 (2015) 25–36.
[6] T. Kaino, K. Jinguji, S. Nara, Low loss poly(methyl methacylate-d8) core optical fibers, Appl. Phys. Lett. 42 (7) (1983) 567–569.
[7] C. Broadway, R. Min, A.G. Leal-Junior, et al., Towardcommercial polymer fiber bragg grating sensors: Review and applications, J. Lightwave Technol. 37 (11) (2019) 2605–2615.
[8] J. Puetz, M.A. Aegerter, Dip coating technique, in: M.A. Aegerter, M. Mennig (Eds.), Sol-Gel Technologies for Glass Producers and Users, Springer, US, 2004, pp. 37–48.
[9] D. Quéré, Fluid coating on a fiber, Annu. Rev. Fluid Mech. 31 (1) (1999) 347–384.
[10] D.A. White, J.A. Tallmadge, A gravity corrected theory for cylinder withdrawal, AIChE J. 13 (4) (1967) 745–750.
[11] D. Grosso, How to exploit the full potential of the dip-coating process to better control film formation, J. Mater. Chem. 43 (21) (2011) 17033–17038.